Functional Materials Letters
Vol. 1, No. 1 (2015) Article number

Fast discharge–charge properties of $FePS_3$ electrode for all-solid-state batteries using sulfide electrolytes and its stable diffusion path

Yuta Fujii, Hiroaki Ito,
Graduate School of Chemical Sciences and Engineering, Hokkaido University, Sapporo, 060-8628, Japan

Akira Miura,* Nataly Carolina Rosero-Navarro, Kiyoharu Tadanaga
Graduate School of Engineering, Hokkaido University, Sapporo, 060-8628, Japan

Li Lu
Department of Mechanical Engineering, National University of Singapore, Singapore, 117575, Singapore

Received Day Month Year; Revised Day Month Year

We report the fast discharge–charge cycle of micro-sized $FePS_3$ electrode particles in all-solid-state batteries using sulfide electrolytes at 80 °C. At a current density of 2.04 mA cm^{-2}, corresponding to approximately 1 C, the capacity of the $FePS_3$ electrodes reached ~180 mAh g^{-1} without any electron or lithium-ion conductive additives. Galvanostatic intermittent titration technique measurements showed a stable diffusion path of $FePS_3$ represented by the product of the diffusion coefficient and square of the surface area. These electrochemical properties were compared with those of FeS, whose capacity was lower because of its unstable diffusion path.

Keywords: Diffusion path, Galvanostatic intermittent titration technique (GITT) measurement, Iron.

* Corresponding author
Email: amiura@eng.hokudai.ac.jp (A. Miura)

Functional Materials Letters
Vol. 1, No. 1 (2015) Article number

1. Introduction

All-solid-state batteries (ASSBs) are considered the next-generation batteries because of their safety and high energy density.[1–3] Sulfide electrolytes are the key materials of ASSBs because they exhibit high lithium mobility and deformability under pressure.[4–6] The cathodes and anodes used in liquid batteries can be utilized for ASSBs with sulfide electrodes; $LiCoO_2$/$Li(Ni,Mn,Co)O_2$ and graphite are used for the cathode and anode, respectively.[1–6] However, the unstable nature of sulfide electrolytes, especially at high voltage (>3 V), and low capacity of cathode materials limit the wide-application of sulfide-electrolyte-based ASSBs.

A sulfur-based cathode operating at low voltage is desirable for use in ASSBs because it can facilitate high capacity (1675 mAh g^{-1})[7]. When using solid electrolytes, sulfur will not be dissolved in the electrolytes, unlike in batteries wherein organic electrolytes are used. Moreover, the operating voltage of the sulfur electrode (2.15 V vs. Li/Li^+) is lower than that of other oxide electrodes (>3 V), which facilitates the use of sulfide electrolytes in applications requiring stable electrochemical windows.

Electrodes exhibiting both ion and electron conductivities are essential to ASSB operation. Lower conductivity would be the rate-limiting factor for operating ASSBs under high current densities. During the discharge and charge processes of sulfur electrodes, the conversion reaction between S and Li_2S occurs together with electron transfer. Because both S and Li_2S are insulators, their electron conductivity should be enhanced for improving the performance of ASSBs.

Two approaches have been proposed to operate Li-S ASSBs, one of which is to mix both electron and ion conductors to form composite electrodes. Typical electron and ion conductive materials are carbon and Li-P-S electrolytes, respectively. Nanocomposite electrodes produced by thoroughly mixing sulfur, carbon and Li-P-S electrolytes have been used in ASSBs.[8–9] Nonetheless, as S and Li_2S are insulators, charge transfer inside sulfur particles is slow even after the addition of a large amount of carbon. As a result, it is difficult to increase the capacity per volume of the composite electrodes, especially at high current densities.

The second approach is to use metal sulfides, which impart higher electron conductivity than that by the aforementioned approach.[10–19] Among metal sulfides, Fe–S-based electrodes are attractive because their components are abundant in nature and inexpensive. For example, FeS is a good candidate for the cathode material when utilized with a carbon additive. ASSBs composed of sulfide electrolytes exhibited a high capacity of >500 mAh g^{-1} (per mass of electrode).[20–21] The reaction mechanism is proposed as follows[20–21]:

$$FeS + Li^+ + e^- \rightleftarrows 1/2\ Li_2FeS_2 + 1/2Fe \qquad \text{Eq. (1)}$$

$$1/2\ Li_2FeS_2 + Li^+ + e^- \rightleftarrows Li_2S + 1/2Fe \qquad \text{Eq. (2)}$$

$$Li_2FeS_2 \rightleftarrows Li_{2-x}FeS_2 + xLi^+ + xe^- \qquad \text{Eq. (3)}$$

$$Li_{2-x}FeS_2 \rightleftarrows FeS_y + (2-y)S + (2-x)Li^+ + (2-x)e^- \qquad \text{Eq. (4)}$$

Discharge–charge cycling involves the oxidation and reduction of sulfur[20–21]; thus, these are at least partially sulfur electrodes. We have studied $FePS_3$ as a cathode for ASSBs[22–23], which has also been utilized in lithium-ion batteries using organic solvents on the basis of the following electrochemical reaction:[24–25]

$$FePS_3 + 1.5\ Li^+ + 1.5\ e^- \rightleftarrows Li_{1.5}FePS_3 \qquad \text{Eq. (5)}$$

Because $FePS_3$ is a conductor of both electrons and lithium ions,[22] $FePS_3$ can be used as the electrode in ASSBs without the requirement of electron and lithium-ion conductive additives although the battery is operated at a current density of 0.1 mA.[22] Non-requirement of electron and lithium-ion conductive additives has the advantage of increasing electrode capacity. Upon discharge–charge cycling, it has been proposed that the oxidation and reduction of sulfur can proceed without destroying the structural framework.[23] Recently, an ASSB using an Fe-P-S electrode operated at 100 °C exhibited a reversible capacity of >625 mAh g^{-1} for 50 cycles at 0.51 mA cm^{-2} (~0.1 C), despite the low carbon content (2 wt%) of the electrode.[26]

To achieve high capacity with high current density, stable diffusion paths of lithium ions and electrons along the entire electrode particle are essential. In this work, the performance of batteries using $FePS_3$ and FeS electrodes in ASSBs was examined, and their diffusion paths were evaluated using the galvanostatic intermittent titration technique (GITT).

2. Experimental

FeS and $FePS_3$ powders were selected and used as Fe–S-based electrode active materials. $FePS_3$ was prepared by heating iron (Wako Chemical, 99.9%), red phosphorus (Kanto Chemical, 98.0%), and sulfur (Kanto Chemical, 99.5%) in an evacuated quartz tube according to previous reports.[22,23] To collect powders with uniform particle size, FeS (Mitsuwa Chemical, $Fe_xS(0.9 \leqq x \leqq 1)$) and the prepared $FePS_3$ powders were ground using an agata mortar,

and particles larger than 38 µm were removed using a 38 µm sieve. $FePS_3$ (0.5 g) and FeS (1.2 g) were placed in ZrO_2 pots (45 mL) with 20 ZrO_2 balls (4 mm in diameter). The powders were ball-milled at a rotation speed of 150 rpm for 12 or 48 h to further decrease the particle size. X-ray diffraction (XRD) patterns of the two obtained powders were recorded using an X-ray diffractometer (MiniFlex600, Rigaku) with a CuKα radiation source. The morphologies of these powders were investigated through scanning electron microscopy (SEM; TM3030Plus, Hitachi-High-Tech). The electronic conductivities of $FePS_3$ and FeS were measured via the conventional two-terminal method by pressing the powders between two metal rods in an insulating tube at room temperature.

ASSBs (Li-In/$75Li_2S{\cdot}25P_2S_5$ (mol%) glass/Fe–S based electrodes) were fabricated according to a previously reported method.[1] In typical processing, a $75Li_2S{\cdot}25P_2S_5$ glass solid electrolyte was prepared by mechanical milling of a mixture of Li_2S (Mitsuwa Chemical, 99.9%) and P_2S_5 (Aldrich, 99%).[27] The cathodes were prepared using only Fe–S-based electrode active materials (FeS_x and $FePS_3$) or mixtures of the Fe–S-based materials with $75Li_2S{\cdot}25P_2S_5$ glass and vapor-grown carbon fibers (VGCF, Showa Denko). The volume ratio of the Fe–S electrode:$75Li_2S{\cdot}25P_2S_5$ glass:VGCF in the composite cathodes was 50:45:5. The prepared cathodes (10 mg) and $75Li_2S{\cdot}25P_2S_5$ glass solid electrolytes (120 mg) were placed into polycarbonate tubes (φ = 10 mm). Bilayer pellets were obtained by pressing at 360 MPa. A Li-In alloy foil was used as the counter electrode and pressed under 120 MPa. The obtained pellets were sandwiched between two stainless steel disks as current collectors. The ASSBs using only the Fe–S-based electrode active materials (10 mg of FeS and $FePS_3$) as the cathode without solid electrolytes and conductive additives were discharged and charged using a discharge–charge measuring station (Scribner Associates, 580 battery-type system) at a constant current density of 2.04 mA cm^{-2} at 25 to 80 °C. In order to evaluate the diffusion path, GITT measurements were performed.[28–29] The current pulse and relaxation at open circuit were respectively set to 0.13 mA cm^{-2} and 90 min in each step. The fabrication of the ASSBs and electrochemical measurements using the batteries were carried out in a dry Ar atmosphere.

3. Results

The XRD patterns of $FePS_3$ and FeS suggested the presence of single-phase materials without impurities (Figure 1(a)). Both particles exhibit similar morphologies (Figure 1(b,c)); thus, there is no significant difference in their surface area. The electronic conductivities of the $FePS_3$ and FeS pellets were 4×10^{-5} and $>3.1\times10^{-1}$ S cm^{-1}, respectively, at room temperature.

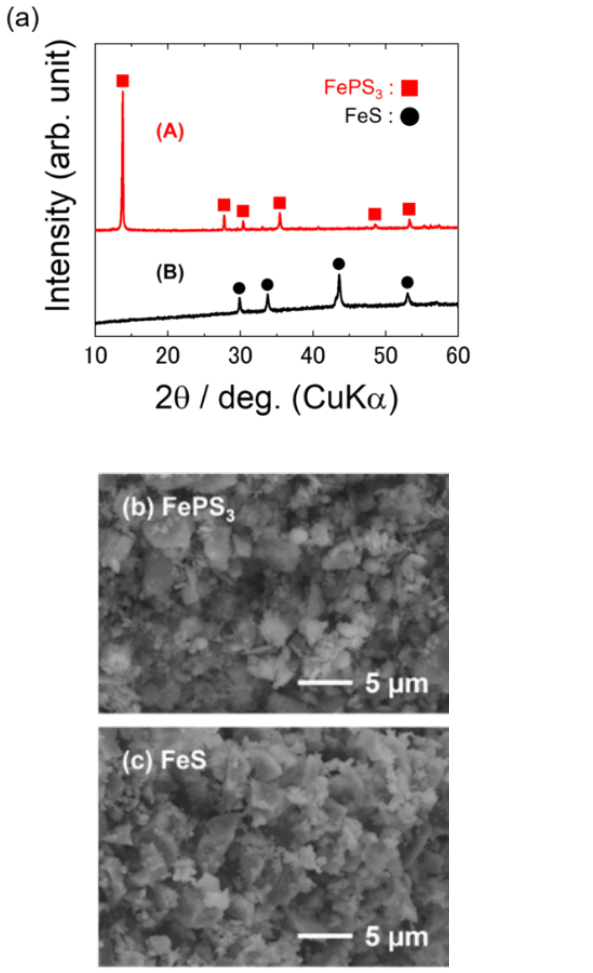

Figure 1. (a) XRD patterns of $FePS_3$ and FeS electrodes and (b) and (c) corresponding SEM images.

The discharge–charge properties of $FePS_3$ without electron or lithium-ion conductive additives were examined at a current density of 2.04 mA cm^{-2}, corresponding to approximately 1 C for $FePS_3$. At 25 °C, only negligibly low capacity was observed (Figure 2 (a)). At 80 °C, the capacity significantly increased to ~180 mAh g^{-1}. Considering the electrode with no lithium-ion and electron additives, $FePS_3$ itself possesses sufficient lithium-ion and electron conduction for 1 C discharge–charge cycling. The capacity of $FePS_3$ at 25 °C is comparable to that of FeS electrodes, while that at 80 °C is higher.

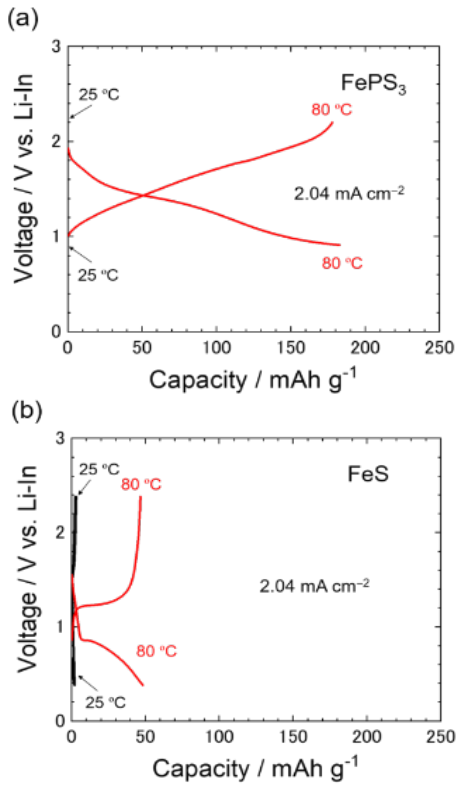

Figure 2. Discharge–charge curves of the 3rd cycle of an ASSB using (a) $FePS_3$ and (b) FeS electrodes at 25 and 80 °C, where the cut-off voltage of the ASSB using the $FePS_3$ electrode was set to 0.91 V vs. Li-In for discharging and 2.2 V vs. Li-In for charging, whereas for the battery using an FeS electrode, the cut-off voltage was set to 0.38 V vs. Li-In for discharging and 2.38 V vs. Li-In for charging. The voltage vs. Li-In was 0.6 V lower than the voltage vs. Li.

To study diffusion in the electrode particles, the electrode for the GITT study was mixed with Fe–S electrodes, $75Li_2S{\cdot}25P_2S_5$ glass, and VGCF in a volume ratio of 50:45:5 (vol%) so that both $FePS_3$ and FeS particles could have sufficient lithium-ion diffusion and electron conduction paths on the surface. The GITT profiles shown in Figure 3 reveal higher capacities because of the low current density and the addition of the lithium-ion electrolyte and an electron conductor. The current pulse and relaxation for the open circuit were set to 0.13 mA cm^{-2} and 90 min, respectively, in each step. The GITT measurements allowed for the estimation of the diffusion coefficient based on the following equation:[28–29]

$$D = \frac{1}{2}\left(V_M \frac{\delta E_S/\delta x}{SFA_W}\right)^2 \qquad \text{E}$$

q. (6)

where D is the diffusion coefficient, V_M is the molar volume, S is the specific electrode surface area, F is Faraday's constant, $\delta E_S/\delta x$ is the slope of equilibrium OCP vs. Li content, and A_W is the Warburg factor. In this work, we characterized the stability of the network of lithium-ion diffusion and electron conduction paths on the basis of the change in the products of the diffusion coefficient and the square of the interface area.

$$DS^2 = \frac{1}{2}\left(V_M \frac{\delta E_S/\delta x}{FA_W}\right)^2 \qquad \text{Eq. (7)}$$

The GITT profile of $FePS_3$ was characterized in an insertion up to 1.5 in the ratios of Li/Fe (Eq. (5)), which is

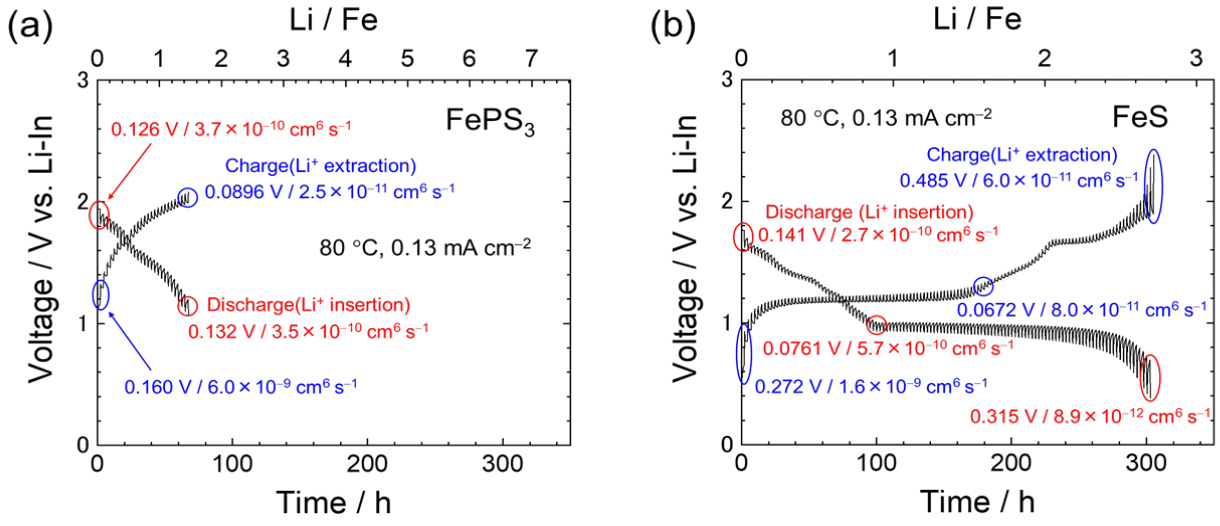

Figure 3. GITT measurements of the ASSB using (a) $FePS_3$ and (b) FeS composite electrodes (Fe-S electrode:$75Li_2S{\cdot}25P_2S_5$ glass:VGCF=50:45:5 (vol%)) at 80 °C. The Li/Fe ratio was calculated from the total of pulse currents. The iR drop and the product of diffusion coefficient and square of interface area (eq.7) are denoted. The voltage vs. Li-In was 0.6 V lower than the voltage vs. Li.

considered as the limit of intercalation of Li^+ into $FePS_3$.[23] Before and after Li^+ insertion, there are no significant changes in the iR drop (0.126 V and 0.132 V, respectively) and the diffusion path represented as the product of the diffusion coefficient and square of the interface area (eq. 7), indicating a stable diffusion path. During charging, the iR drop reduced by half, and the product of the diffusion coefficient and square of the interface area increased in comparison to that upon stable Li^+ insertion. This is likely attributed to the destruction of the Li^+ diffusion path from less-lithiated $FePS_3$. Nonetheless, these changes are less significant than those found in FeS on Li^+ extraction, as described below.

The GITT profile of FeS is shown in Figure 3 (b). Two-step discharge profiles (>0.9 V and <0.9 V) can be seen. As reported, the first step at approximately >0.9 V is attributed to the intercalation reaction presented in Eq. (3), while the second step at approximately <0.9 V is attributed to the conversion reaction as indicated by Eq. (4).[21] During intercalation, lithium-ion insertion reduced the iR drop and increased the product derived by GITT analysis, indicating that the diffusion path changes upon lithium-ion insertion. Further lithium-ion insertion in the conversion reaction significantly increased the iR drop and decreased the product derived by GITT analysis, indicating a significant change in diffusion mechanisms. This is probably related to the formation of insulating Li_2S (Eq. (2)), which blocks electron paths. At the beginning of charging, the iR drop decreases and becomes stable in the plateau at 1.2 V. This stable plateau can be attributed to the extraction of Li^+ from Li_2FeS_2 (Eq. (2)) with high electronic conductivity (~10^{-1} S cm^{-1}).[30] iR drop one-order increased in the later stage. On the other hand, the product of the diffusion coefficient and square of the interface area approximately two-order decreased in the beginning and slightly decreased in the later stage. Again, the changes in the iR drop and the product during Li^+ extraction are larger than those found in $FePS_3$, presumably related to its multi-step reaction mechanism.[20–21]

4. Conclusions

This work demonstrates the advantage of $FePS_3$ as an electrode for ASSBs that can operated in the absence of electron and lithium-ion conductive additives. A capacity as high as 180 mAh g^{-1} at a high current density of 2.04 mA cm^{-2} (~1 C) was achieved at 80 °C, indicating that high temperature facilitates stable electron conduction and lithium-ion diffusion paths for successful lithium-ion migration. Compared with the capacity at room temperature, as shown in Figure 2 and our previous work, the capacity determined in this study has significantly increased. Furthermore, the stability of the electron and lithium-ion paths at 80 °C is demonstrated by a slight change in the products of the diffusion coefficient and the square of the interface area achieved by GITT analysis.

5. Acknowledgments

This work was partially supported by the Japan Science and Technology Agency (JST), Advanced Low Carbon Technology Research and Development Program (ALCA), Specially Promoted Research for Innovative Next Generation Batteries (SPRING) project, and Grant-in-Aid for JSPS Research Fellow (18J11169).

6. References

1. M. Tatsumisago *et al.*, Recent development of sulfide solid electrolytes and interfacial modification for all-solid-state rechargeable lithium batteries, *J. Asian Ceram. Soc.* **1 (1)**, 17 (2013).
2. M. Shoji *et al.*, Recent progress for all solid state battery using sulfide and oxide solid electrolytes, *J. Phys. D: Appl. Phys.* **52** (10), 103001 (2019).
3. S. Xia *et al.*, Practical Challenges and Future Perspectives of All-Solid-State Lithium-Metal Batteries, *Chem* **5 (4)**, 753 (2019).
4. A. Manthiram *et al.* Lithium battery chemistries enabled by solid-state electrolytes, *Nat. Rev. Mat.* **2 (4)**, (2017).
5. A. Miura *et al.*, Liquid-phase syntheses of sulfide electrolytes for all-solid-state lithium battery, *Nat. Rev. Chem.* **3**, 189 (2019).
6. J. Lau *et al.*, Sulfide Solid Electrolytes for Lithium Battery Applications, *Adv. Energy Mater.* **8 (27)**, 1800933 (2018).
7. A. Manthiram *et al.*, Challenges and Prospects of Lithium–Sulfur Batteries, *Acc. Chem. Res.* **46 (5)**, 1125 (2013).
8. M. Nagao *et al.*, Sulfur–carbon composite electrode for all-solid-state Li/S battery with Li_2S–P_2S_5 solid electrolyte, *Electrochim. Acta* **56 (17)**, 6055 (2011).
9. T. Hakari *et al.*, All-solid-state lithium batteries with Li_3PS_4 glass as active material, *J. Power Sources* **293**, 721 (2015).
10. A. Hayashi *et al.*, Amorphous Titanium Sulfide Electrode for All-solid-state Rechargeable Lithium Batteries with High Capacity, *Chem. Lett.* **41 (9)**, 886 (2012).
11. T. Matsuyama *et al.*, Electrochemical properties of all-solid-state lithium batteries with amorphous MoS_3 electrodes prepared by mechanical milling, *J. Mater. Chem. A* **3 (27)**, 14142 (2015).
12. A. Sakuda *et al.*, Amorphous TiS_4 positive electrode for lithium–sulfur secondary batteries, *Electrochem. Commun.* **31**, 71 (2013).
13. A. Sakuda *et al.*, Composite positive electrode based on amorphous titanium polysulfide for application in all-solid-state lithium secondary batteries, *Solid State Ionics* **262**, 143 (2014).
14. Y. Suto *et al.*, Synthesis of submicron-sized $NiPS_3$ particles and electrochemical properties as active materials in all-

solid-state lithium batteries, *J. Ceram. Soc. Jpn.* **126 (7)**, 568 (2018).
15. H. Wan *et al.*, Transitional Metal Catalytic Pyrite Cathode Enables Ultrastable Four-Electron-Based All-Solid-State Lithium Batteries, *ACS Nano* **13 (8)**, 9551 (2019).
16. M. Pan *et al.*, Electrochemical Properties of All-solid-state Lithium Batteries with Amorphous FeS_x-based Composite Positive Electrodes Prepared via Mechanochemistry, *Electrochemistry* **86 (4)**, 175 (2018).
17. U. Ulissi *et al.*, High Capacity All-Solid-State Lithium Batteries Enabled by Pyrite-Sulfur Composites. *Adv. Energy Mater.* **8 (26)**, 1801462 (2018).
18. Y. Fujii *et al.*, Development of All-solid-state Lithium Secondary Batteries Using $NiPS_3$ Electrode and Li_2S-P_2S_5 Solid Electrolyte, *Chem. Lett.* **45 (6)**, 652 (2016).
19. Y. Kawasaki *et al.*, Synthesis and Electrochemical Properties of Li_3CuS_2 as a Positive Electrode Material for All-Solid-State Batteries, *ACS Appl. Energy Mater.*, in press.
20. Q. Zhang *et al.*, FeS nanosheets as positive electrodes for all-solid-state lithium batteries, *Solid State Ionics* **318**, 60 (2018).
21. T. Yersak *et al.*, Solid State Enabled Reversible Four Electron Storage, *Adv. Energy Mater.* **3 (1)**, 120 (2013).
22. Y. Fujii *et al.*, $FePS_3$ electrodes in all-solid-state lithium secondary batteries using sulfide-based solid electrolytes, *Electrochim. Acta* **241**, 370 (2017).
23. Y. Fujii *et al.*, Reaction Mechanism of $FePS_3$ Electrodes in All-Solid-State Lithium Secondary Batteries Using Sulfide-Based Solid Electrolytes, *J. Electrochem. Soc.* **165 (13)**, A2948 (2018).
24. Y. V. Kuzminskii *et al.*, Iron and nickel phosphorus trisulfides as electroactive materials for primary lithium batteries, *J. Power Sources* **55 (2)**, 133 (1995).
25. M. Wang, K. Tang, A facile synthesis of $FePS_3$@C nanocomposites and their enhanced performance in lithium-ion batteries, *Dalton Trans.* **48 (12)**, 3819 (2019).
26. Y. Fujii *et al.*, Fe–P–S electrodes for all-solid-state lithium secondary batteries using sulfide-based solid electrolytes, *J. Power Sources* **449**, 227576 (2020).
27. A. Hayashi *et al.*, Preparation of Li_2S–P_2S_5 Amorphous Solid Electrolytes by Mechanical Milling, *J. Am. Ceram. Soc.* **84 (2)**, 477 (2001).
28. W. Weppner, R. A. Huggins, Determination of the Kinetic Parameters of Mixed-Conducting Electrodes and Application to the System L_3Sb, *J. Electrochem. Soc.* **124**, 1569 (1977).
29. P. F. Xiao *et al.*, Transport and electrochemical properties of high potential tavorite $LiVPO_4F$, *Solid State Ionics* **242**, 10 (2013).
30. S. P. S. Badwal *et al.*, Conductivities and Electronic Structures of Some Phases in the Lithium-Iron-Sulfur System, J. Solid State Chem. **43**, 163 (1982).